# Errors in Hypocenter Location:
# Picking, Model, and Magnitude Dependence

by S. D. Billings, M. S. Sambridge, and B. L. N. Kennett

**Abstract** The location procedures of seismic events are influenced by two major classes of errors, the error in picking individual seismic phases and modeling error due to the departure of the real Earth from the reference model used in the location. Both classes of error influence the estimate of location and it is difficult to separate them.

The role of picking errors can be assessed by a nonlinear analysis using a Monte Carlo procedure. Arrivals times are perturbed with random numbers drawn from a normal distribution, and the event is relocated using these perturbed arrival times. By repeating the procedure many times, a cluster of locations is obtained, which can be used to investigate the effects of picking errors on the hypocenter. This analysis is insensitive to velocity-model errors as these are fixed for a given combination of stations and phases. Some care must be exercised when analysing multidimensional distributions in two-dimensional slices because of a projection effect.

The modeling error due to the influence of lateral heterogeneity in the Earth is examined by comparing the locations of the same event using different combinations of phases and network geometries, which reinforces the need to use arrivals other than $P$ for accurate depth resolution. The sensitivity of $P$ arrivals to changes in depth are swamped by model errors, and inclusion of depth-sensitive phases such as $pP$ is highly recommended. The effect of picking errors on location is found to be much smaller than the mislocation caused by neglecting lateral heterogeneity when only $P$ arrivals are used. Consequently, the Monte Carlo analysis, which is primarily aimed at picking errors only, is most appropriate when multiple phases have been used to more accurately constrain the hypocenter, especially for the depth component.

Altering the type of phase data used in the location plays a similar role in changing the network geometry, in that both are mechanisms that influence the nature of the constraint on the hypocenter. By relocating events with network geometries corresponding to the different magnitudes, it is found that the location of the event can be affected significantly by the magnitude, and when using robust statistics to describe earthquake residuals, the mislocation can occur in a systematic manner. The effect is marked in regions with significant lateral variations in seismic velocities. For example, low-magnitude events in the Flores Sea are found to be dragged toward Australia as a result of the fast paths to Australian stations relative to the *iasp*91 reference velocity model.

## Introduction

An inverse problem usually involves inverting data for a series of model parameters describing a real system. A *forward model* is derived that converts a realization of the system into a set of calculated data. A *misfit criterion* is then specified that measures the discrepancy between the calculated and real data. The solution of the inverse problem is often defined as that particular parameterization of the system that yields predictions that are *most consistent* with the real data. Inadequacies in the data, the forward model, and the parameterization lead to this computed solution differing from the real solution. For earthquake locations, the data

consist of imperfectly measured arrival times of seismic waves at a number of locations around the globe, while the forward model specifies a method for computing arrival times from an arbitrary source to an arbitrary receiver. Usually, this involves tracing rays through a one-dimensional approximation of the Earth, which introduces errors due to the neglect of the effects of lateral velocity variations.

Error analysis is required to assess the reliability of any solution found using an inverse method. Previous treatments of hypocentral errors are inadequate, either because of a linearized analysis of the statistics (Flinn, 1965; Pavlis, 1986), or because of limited statistical treatments of either, or both, sources of error (Tarantola and Valette, 1982). In this article, a Monte Carlo analysis has been used to determine how the hypocenter moves under the influence of errors in picking. Arrival times are perturbed from random numbers drawn from an appropriate distribution and the hypocenter is relocated using these perturbed arrival times. If the procedure is repeated many times, the distribution of perturbed locations can be used to analyze the reliability of the calculated earthquake location. The analysis is sensitive to picking errors only, as the systematic errors in location arising from inadequacies of the velocity model are fixed with a fixed geometry and choice of phases.

The existence of the systematic component can be exposed by comparing the result for the same event with different phase choices, or with different network geometries. The number and type of phases used in a location procedure can have a large effect on the hypocenter, especially in depth. In particular, depth estimates can be significantly in error when $P$ arrivals only are used. We examine this factor by comparing the location found using $P$ arrivals only to a location found using both $P$ and $pP$ arrivals, for the same event. The effect of earthquake magnitude on mislocation is assessed by relocating an event using different network geometries. The distribution of stations in each network is chosen to reflect a global network that would detect events of differing magnitudes from the same epicentral region. The systematic bias introduced into the event location is magnitude dependent and in effect is a result of ignoring lateral variations in velocity when using a one-dimensional velocity model to calculate travel times.

The error analysis presented in this article is designed for use with nonlinear location algorithms such as genetic algorithms and simulated annealing (Kennett and Sambridge, 1992; Sambridge and Gallagher, 1993; Billings *et al.*, 1994; Billings, 1994). Such algorithms do not suffer from the instability problems of linearized location routines and are easily able to incorporate multiple-phase and array data. The additional constraints provided by these data lead to the final locations being more accurate than inversions based on just the first arrival times of $P$ waves. All analysis here is performed

with the simulated annealing algorithm described in Billings (1994), which has been shown to reliably locate earthquake hypocenters. The one-dimensional *iasp*91 velocity model of Kennett and Engdahl (1991) is used to calculate travel times.

## Measurement and Velocity-Model Errors

Most earthquake location algorithms, including the simulated annealing algorithm of Billings (1994), use a maximum likelihood approach. In this method, one finds the hypocenter $\underline{\mathbf{h}} = (x, y, z, t)$ with maximum *posteriori* probability, given the observed arrival times $t^{arr}$ and some assumptions about the nature of the error statistics. This can be achieved by maximizing the conditional probability $P(t^{calc}/t^{arr})$, which from Bayes' rule (Hoel, 1971, p. 20.) is given by

$$P(t^{calc}/t^{arr}) = \frac{P(t^{arr}/t^{calc}) P(t^{calc})}{P(t^{arr})}, \tag{1}$$

where $t^{calc} = t^{calc}(x, y, z, t)$ is the arrival time calculated from the hypocenter $\underline{\mathbf{h}}$, $P(t^{calc})$ is the *a priori* joint probability density function (pdf) of the parameters, and $P(t^{calc})$ is a function independent of $t^{calc}$ that serves as a normalizing factor so that the conditional probability $P(t^{calc}/t^{arr})$ integrates to unity. The only *a priori* information independent of the data is that the depth of focus is below the Earth's surface. Equation (1) can be used to calculate the probability density function of hypocentral position given an assumed pdf of travel-time residuals. Assuming the maximum likelihood point is $\hat{h}$, confidence ellipses can be computed via

$$(h - \hat{h})^T C_h^{-1} (h - \hat{h}) \leq k_\alpha^2, \tag{2}$$

where $C_h = A^+ C (A^+)^T$, $C =$ covariance $(r)$, and $A^+$ is the pseudo inverse (Lawson and Hanson, 1974, pp. 36–40) of the matrix of partial derivatives evaluated at the proposed solution. The value of $k_\alpha$ depends upon the distribution of residuals, $r_i$ ($= t_i^{calc} - t_i^{arr}$, for the $i$th datum), and the confidence level specified. For example, for a normal distribution with zero mean and variance $\sigma^2$, $k_\alpha$ for the $\alpha = 95\%$ confidence level is given by $k_\alpha^2 = 9.488\sigma^2$, where 9.488 is the 95% confidence level for a $\chi^2$ distribution with four degrees of freedom.

Confidence levels calculated using equation (2) assume that the residuals follow a distribution that is adequately modeled by a single error distribution. However, for earthquake location, the residual distribution is better represented by considering two different sources of error; viz. picking and velocity-model errors. In particular, reference velocity models are one-dimensional (1D) approximations to the real Earth's three-dimensional (3D) velocity structure.

Errors in picking are mostly random in character. For impulsive arrivals measured from analog records, the errors are approximately Gaussian (Buland, 1976). For emergent arrivals, the errors have a distribution skewed toward positive numbers as a result of the tendency to pick weak arrivals too late (Anderson, 1982). Velocity-model errors include both random and systematic components. The random errors tend to result from unmodeled short-range velocity structure (Leaver, 1984), while the systematic bias is largely due to unmodeled velocity structure on a long wavelength scale (Jordan and Sverdrup, 1981; Pavlis and Hokanson, 1985).

Flinn (1965) attempted to account for both picking and velocity-model errors in computing the confidence levels by scaling the data covariance $C$ in equation (2) by the root mean square (rms) residuals. Given $n$ travel-time arrivals,

$$ C = s^2 I, \quad \text{where } s^2 = \frac{1}{(n-4)} \left( \frac{1}{n} \sum_{i=1}^{n} r_i^2 \right)^{1/2}, \quad (3) $$

and where $I$ is the identity matrix. The scaling of $C$ is supposed to take account of velocity-model errors. Assuming that picking and velocity-model errors are both normally distributed,

$$ k_\alpha^2 = 4s^2 F_\alpha(4, n-4), \quad (4) $$

where $F_\alpha(4, n-4)$ is an $F$ statistic with 4 and $m-4$ degrees of freedom for the critical level $\alpha$ (see Feldman and Fox, 1991). Evernden (1969) found that as the number of observations, $n$, becomes small, the confidence ellipsoids calculated using equation (4) are unrealistically large. Jordan and Sverdrup (1981) overcame this problem by modifying equation (4) so as to take account of a priori information on the residual distribution:

$$ k_\alpha^2 = \frac{4K + 4s^2(n-4)}{K + (n-4)} F_\alpha(4, K + n - 4). \quad (5) $$

$K$ is a parameter that controls the amount of a priori information. For $K = 0$, Flinn's (1965) analysis is retained, while for $k = \infty$ it is assumed that there is exact prior information (Evernden, 1969). Jordan and Sverdrup (1981) recommend a value of $K = 8$. Analysis using equation (5) in place of equation (4) decreases the size of the confidence limits appreciably when $n$ is small, but has little effect when $n$ is large. Using either equation gives a linearized confidence region that supposedly has the same statistical form as the exact confidence regions in a sufficiently small region around the epicenter, where 10 to 20 km is sufficiently small.

Tarantola and Valette (1982) performed a fully nonlinear analysis of the probability density function in the region of interest. They explicitly separated the errors due to the velocity model and those due to picking. Using $\underline{m} = (X, Y, Z, T)$ and $\underline{t} = (t_1^{arr}, \ldots, t_n^{arr})$, the a posteriori probability density function of the model parameters (hypocentral coordinates), $\sigma_m(\underline{m})$, is

$$ \sigma_m(\underline{m}) = p_m(\underline{m}) \int_T d\underline{t} \frac{p_t(\underline{t}) \, \theta(\underline{t}/\underline{m})}{\mu_t(\underline{t})}, \quad (6) $$

where $p_m(\underline{m})$ is the a priori information on the model parameters, $p_t(\underline{t})$ is the a priori information on data, $\theta(\underline{t}/\underline{m})$ is the probability density function of errors in the velocity model, and $\mu_t(\underline{t})$ is the noninformative density function describing the state of null information. Tarantola and Valette (1982) assume that both picking and velocity-model errors are normally distributed. Denoting the observed arrival times by $\underline{t}_0$ with covariance matrix $C_t$ and the calculated travel times by $\mathbf{h}(X, Y, Z)$ with covariance $C_T$, the a posteriori probability density function for the spatial coordinates is given by

$$ \sigma(X, Y, Z) = K \, p(X, Y, Z) \exp\left[ -\frac{1}{2} [\hat{\underline{t}}_0 - \hat{\mathbf{h}}(X, Y, Z)^T \right. $$

$$ \left. P[\hat{\underline{t}}_0 - \hat{\mathbf{h}}(X, Y, Z)] \right], \quad (7) $$

where $\hat{\underline{t}}_0$ is the observed arrival time minus the weighted mean of the observed arrival times, $\hat{\mathbf{h}}$ is the calculated travel time minus the weighted mean of calculated travel times, $P = (C_T + C_t)^{-1}$, and $K = \Sigma_{ij} P_{ij}$.

Equation (7) can be used to compute the a posteriori density function over the region of interest by evaluating $\sigma(X, Y, Z)$ on a fine grid. The error analysis is fully nonlinear and takes account of the two sources of error. However, the method is expensive to implement in practice and is computationally infeasible for events with more than a few observations. In addition, it can become difficult to use when errors are not normally distributed, e.g., because of interaction of picking and modeling errors.

Pavlis (1986) found that it may not be adequate to treat the velocity-model errors as drawn from a Gaussian distribution with zero mean and that under this assumption, misleading results can be obtained. From a synthetic test using 53 events, Pavlis (1986) found that the velocity models are bimodal and far from Gaussian. As an alternative to considering velocity-model errors as random, Pavlis obtains an upper bound on the size of these errors, by comparing the ray path and slowness in the real Earth to the ray path and slowness in the Earth model. Measurement errors are treated statistically, and assumed to be normally distributed. However, this is unattractive for our purposes, as it relies on a linearized treatment of error analysis. Davies (1992) has ap-

proached the problem from a novel statistical viewpoint and produced lower bounds on average earthquake mislocation using travel-time residuals from many events taken together.

## Nonlinear Analysis of the Effects of Picking Errors

In an inversion, there are usually many arrival times with picking errors that can be treated as approximately normally distributed with zero mean and variance $\sigma^2$. Most previous authors have computed linearized confidence limits. The approach of Tarantola and Valette (1982) discussed above is a notable exception. A fully nonlinear method for error analysis requires a Monte Carlo analysis. The usual procedure is to generate synthetic arrival times from the hypocentral solution produced by the inversion technique. The synthetic data are then perturbed by random noise drawn from the same probability distribution used to locate the original event, and the event is subsequently relocated using these perturbed observations. If a sufficient number of relocations are performed, the relocated events can be used to give a fully nonlinear treatment of the errors with confidence limits calculated by considering the density of relocated points. In this work, we use a Monte Carlo procedure to analyze the effect of picking errors only. This is achieved by using a variation of the standard technique. Instead of generating synthetic arrival times, we add "measurement" noise to the actual observed arrival times and relocate. In this way, the effect of velocity model errors will be present in both the real and perturbed data locations, and so the change in location will be representative of the effect of picking errors alone.

Here we choose to model the *P*-wave arrival picking errors by drawing noise from a Gaussian distribution with zero mean and a standard deviation of 0.25 sec (This represents an accepted error level for picking of *P* waves. For other phases, a larger standard deviation is used, e.g., 0.5 sec for *S* arrivals.) When array observations are included, errors in azimuth and slowness can also be considered by perturbing their values with random numbers drawn from a normal distribution with appropriate standard deviation. Considering only travel-time arrivals and denoting the *i*th random perturbation by $e_i$, the *i*th calculated arrival $t_i^{calc}$, is perturbed to

$$t_i^{calc} \rightarrow t_i^{calc} + e_i. \qquad (8)$$

In the standard Monte Carlo analysis, the distribution used to perturb the synthetic data is the same as that used to locate the original event and relocate the perturbed events. A modified procedure used here as the distribution of residuals is a result of the interaction of two sources of error; viz., time picking and velocity-model errors. The picking errors are adequately described by a

Gaussian distribution, but the combination of both types of errors is better represented by some other statistical distribution. Following Kennett (1992), this distribution is taken to be a generalized Gaussian,

$$P(t^{arr}/t^{calc}) = A \exp\left[\frac{-1}{p} \sum_{i=1}^{n} \frac{|t_i^{calc} - t_i^{calc}|^p}{\sigma_i^p}\right], \qquad (9)$$

where the constant $A$ ensures that equation (9) integrates to unity, and $p$ determines the shape of the distribution. Here, $p$ will be taken to be equal to 1.25, which produces a distribution that approximately mimics the actual residual distribution, and is robust, in the sense that the influence of large residuals are down weighted. Perturbing the arrival times with random numbers drawn from a distribution associated with an $L1.25$ norm would be inappropriate, as this would assume that the picking errors follow an $L1.25$ distribution, and hence, are not normally distributed. Consequently, the data are perturbed using a Gaussian distribution, but the event is relocated using an $L1.25$ norm.

Location of all perturbed and unperturbed hypocenters is achieved using the simulated annealing location algorithm of Billings (1994) based on the method described by Kirkpatrick *et al.* (1983). The algorithm iteratively improves on a random initial starting location by a process analogous to the thermodynamic cooling of particles in a heat bath (Metropolis *et al.*, 1953). If the temperature of the heat bath is lowered sufficiently slowly, the state of minimum energy, which corresponds to a perfect crystalline solid, is achieved. In an optimization problem, the object is to reach the globally minimal state. For earthquake location, this involves minimizing the misfit,

$$\phi = \sum_{i=1}^{n} \frac{|t_i^{calc} - t_i^{calc}|^p}{\sigma_i^p}, \qquad (10)$$

over the four hypocentral coordinates. The iterative process is halted when some termination criterion is reached, which here is taken as 50 iterations without improvement to the best model. The algorithm is nonlinear as no derivative calculations are required, and it has the potential to escape from local minima by occasionally accepting states that increase misfit. Billings (1994) shows that the simulated annealing algorithm can rapidly and accurately locate earthquake hypocenters using any combination of phase and array data.

Location of perturbed hypocenters can be achieved even faster by using the unperturbed hypocenter as the initial model and focusing attention on regions close to the perturbed model, since we do not expect picking errors to move the hypocenter by large amounts (e.g., 1°). In a real application, perhaps 15 to 20 relocations would

give an idea as to how the errors in measurement affect the hypocentral location. However, for a more thorough investigation, of the order of 500 relocations would be appropriate.

### Effect of Picking Errors on a Real Event

To investigate the effects of picking error, we use an event on the Iran/Iraq border (see Table 1). For this event, a total of 307 observations were reported to the ISC. Of these, 38 observations (31 $P$ and seven $pP$) with evenly distributed azimuths were selected for the present study (see Fig. 1). The event was first analyzed using only $P$ arrival times. Figure 2 displays 500 perturbed locations projected onto four planes through the unperturbed hypocenter (with misfit contours superimposed, see later). The perturbed locations all differ by less than 4.5 km in epicenter, 6 km in depth, and 0.75 sec in origin time. These figures represent the uncertainty introduced by picking errors alone. The noise added to the real arrival times has a Gaussian distribution with a zero mean and 0.25-sec standard deviation. We note that depth and origin time are strongly correlated, reflecting the often observed trade-off between these two coordinates. The only noticeable correlation between spatial coordinates occurs with latitude and depth.

A quantity that can easily be calculated is the misfit of a location, which allows us to construct the misfit surface. This surface essentially describes the *a posterior* probability density function, as the misfit is represented by equation (10), while the *a posterior* pdf represents the negative exponential of this quantity (equation 9). Consequently, low misfit values correspond to high values of the *a posterior* pdf, and vice versa. An important question is how the perturbed locations correspond to the structure of the *a posterior* pdf and hence the misfit surface. The misfit contours are shown in Figure 2 and define approximately elliptical shapes, with the depth and origin time strongly correlated. One can see in Figure 2 that the contours of the misfit surface are not oriented in the same direction as the trend in the perturbed locations. This feature is more evident in Figure 3, which shows a similar set of perturbed solutions, using both $P$ and $pP$ data in the location. The nonalign-

ment of perturbed locations and misfit contours is especially noticeable in the latitude-depth and longitude-depth planes.

There are two factors contributing to this nonalignment. The first is that the misfit contours in Figures 2 and 3 correspond to the distribution used to locate the events; i.e., an $L1.25$. However, the noise used to simulate picking errors follows a Gaussian distribution and so one would not necessarily expect the perturbed solutions to follow the contours describing the $L1.25$ distribution, even though the latter is used as the misfit function in the relocation. The second reason is that Figures 2 and 3 represent the projections of four-dimensional points onto two-dimensional planes, whereas the contours are the intersections of the four-dimensional contour surface with the plane, and these will not necessarily be coincident. This would be true even if all the distributions were Gaussian. This *projection effect* is illustrated in Figure 4, which shows an ellipsoidal surface with constant misfit value intersecting an arbitrary plane. Similar ellipsoids with other misfit values will each cut the plane in elliptical contours, defining a contour map of misfit values in the plane. The perturbed locations will be distributed out of the plane and follow the slope of the ellipsoid. Clearly, the projection of the ellipsoid onto the arbitrary plane, and hence, the projection of the perturbed locations, produces the shadowed region, and in general, this will not be aligned with the contours of the misfit function in the plane.

In Figure 3, the projection effect is most prominent when the out of plane direction is the origin time. In Figure 5, we plot those locations that have an origin time 0.3 or more seconds larger than the origin time of the unperturbed location with dark triangles, and those with locations that are 0.3 or more seconds less as light triangles. Locations with origin times in between are shown by crosses. It can be seen that most outlying points lie significantly above, or below, the reference plane. Ignoring these points brings the perturbed locations into better alignment with the misfit contours, and so the projection effect seems to be mainly responsible for the nonalignment in the cases studied here. Therefore, care must be exercised when drawing conclusions from two-dimensional projections of multidimensional functions. In

Table 1

ISC Locations and Origin Times of Events Used in the Illustration of the Error Analysis Technique (Number Observed Represents the Total Number of Arrivals Used in the Inversion)

| Event | Latitude | Longitude | Depth | Origin Time | Number Observed |
|---|---|---|---|---|---|
| Iran/Iraq border | 32.7° N | 47.8° E | 40 km | 1988 i 26 09 34 49.6 | 38 |
| Flores (large) | 7.5° S | 120.7° E | 632 km | 1986 iii 21 21 35 37.0 | 190 |
| Flores (medium) | 7.3° S | 120.2° E | 416 km | 1986 iii 24 02 23 25.0 | 118 |
| Flores (small) | 7.3° S | 120.4° E | 400 km | 1986 i 31 06 19 36.1 | 21 |

addition, the example indicates that if the nonalignment effect occurs, it is likely to be because the higher-dimensional misfit surface is inclined steeply to the projection plane, which indicates that at least one of the out of plane parameters is highly correlated with one of the in plane parameters. In Figures 2 and 3, we notice that it is not prominent when depth and origin time are both in plane or both out of plane. Similar slices of time latitude and time longitude (not shown) also exhibit the effect, and therefore we can conclude that it is primarily a manifestation of the commonly observed trade-off between the origin time and depth parameters.

## Model Errors in Hypocentral Location

### Errors Introduced by Inadequate Combinations of Phases

Model errors can be examined by considering a relocation of the same event using different combinations of phases. Inspection of the epicenter and depth ranges of the error analysis for the locations produced with *P* data only and those produced with *P* and *pP* (Figs. 2 and 3) reveals a large discrepancy. The *P* only depth occurs at around 61 km, while inclusion of *pP* decreases the depth to 26 km, which is closer to the depth found using all phase information (27 km). It appears that the *P* only location is in error by around 12.5 km in epicenter and 35 km in depth; however, Monte Carlo analysis of the picking errors indicated that these errors should affect the *P* arrival location by less than 4.5 km in epicenter and 6 km in depth. The large discrepancy results from imperfections in the velocity model that are compounded by the relative insensitivity of the *P*-wave arrivals to changes in depth at teleseismic distances. Such errors are difficult to analyze, as there is currently no satisfactory method of treating velocity-model errors. It is clearly far better to incorporate multiple phases that provide independent constraint on the location than it is to try a fully nonlinear treatment of picking errors alone.

The *P*-wave arrivals are not very sensitive to changes in depth because of the geometries of the ray paths. Changing depths changes the length of the ray paths by a small amount, and hence has only a small effect on



Figure 1. Station distribution for the Iran/Iraq border event.

the travel time. Consider the travel time to a station from a particular latitude and longitude at two separate depths. For convenience, assume that the two depths are the $P$ and $pP$ (26 km) and the $P$ only (61 km) depths for the Iran/Iraq event. Denote the difference in travel times by $\Delta t^P$. Consider the error in travel time, $\Delta T$, from one of these depths (say 61 km), because of the fact that the ray is traced through a reference velocity model. This error is generally much larger than the difference in travel time when changing depths, i.e., $\Delta T \gg \Delta t^P$. Consequently, the depth sensitivity is swamped by the velocity-model errors. When a depth-sensitive phase such as $pP$ is added, the depth is able to be resolved much more accurately. This arises because changes in the travel time of $pP$ waves when changing depths, $\Delta t^{pP}$, are much larger

than for $P$ waves, $\Delta t^{pP} \gg \Delta t^P$, and perhaps comparable to the velocity-model errors, $\Delta t^{pP} \sim \Delta T$.

The poor depth resolution was investigated on a large number of events with multiple arrivals available. Generally, the depths found including only $P$ and $pP$ arrivals differed little from locations found using multiple arrivals. However, both locations were usually substantially different in depth than the $P$ arrival only location, except when multiple local or regional arrivals of $P$ were available. Previously, Van der Hilst and Engdahl (1993) studied a large number of ISC events and found that the depth estimates for $P$ and $pP$ locations were substantially different from depth estimates based on $P$ arrivals only. The depth bias was particularly evident in subduction zones where there were significant lateral heterogenei-
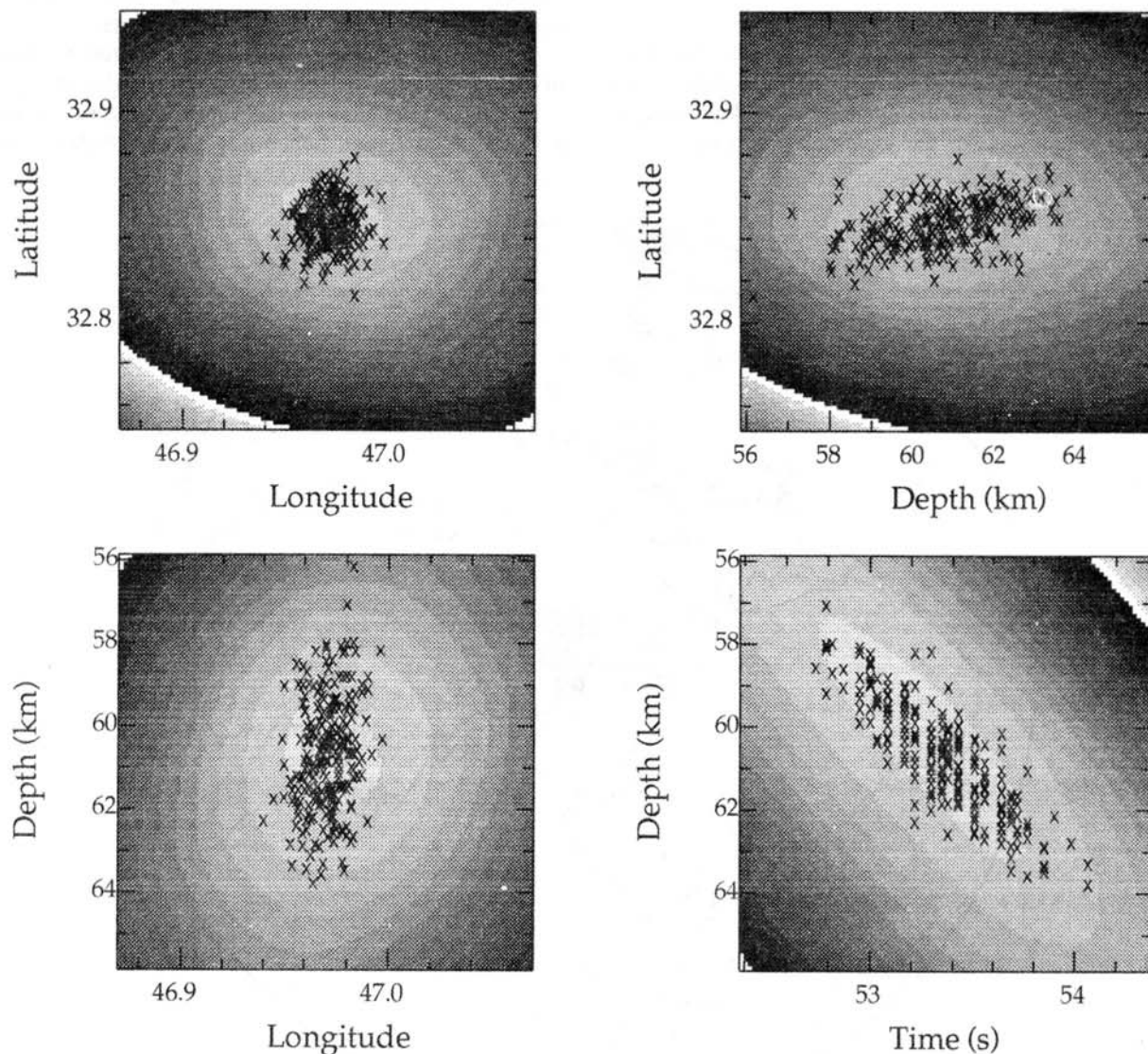


Figure 2.    Distribution of perturbed locations for Iran/Iraq earthquake using only $P$ arrivals, with misfit contours superimposed. The unperturbed location defines the center of each section. Lighter shading indicates lower misfit and hence *better* locations.

ties in seismic velocities. In conclusion, hypocenter location with *P* arrivals alone can lead to large errors in the estimation of depth, which can be partially masked by the inadequacies of a 1D forward model. Even the most sophisticated error anaiysis, based on *P* arrivals only, is unlikely to detect this effect because it is very difficult to adequately incorporate velocity-model errors. Consequently, we would suggest including the maximum amount of phase information, especially depth-sensitive phases such as *pP*.

### Magnitude-Dependent Velocity-Model Errors

The use of a 1D velocity model for the calculation of travel times can also lead to a magnitude dependence of hypocenters in regions where there are significant lateral velocity variations, because the number and pattern of recording stations varies with the magnitude of the event. When a Gaussian misfit function is used, the final location can often be sensitive to a small subset of stations in the locating network, because of the inherent nonrobust dependence on arrival time residuals. When using robust statistical measures, such as the Jeffreys distribution (Jeffreys, 1932; Sambridge and Kennett, 1986), which has been used in the uniform reduction algorithm of the ISC (Adams *et al.*, 1982), an *L*1 norm (Kennett, 1992), or an *L*1.25 norm (Billings, 1994), the location bias can occur in more a systematic manner.

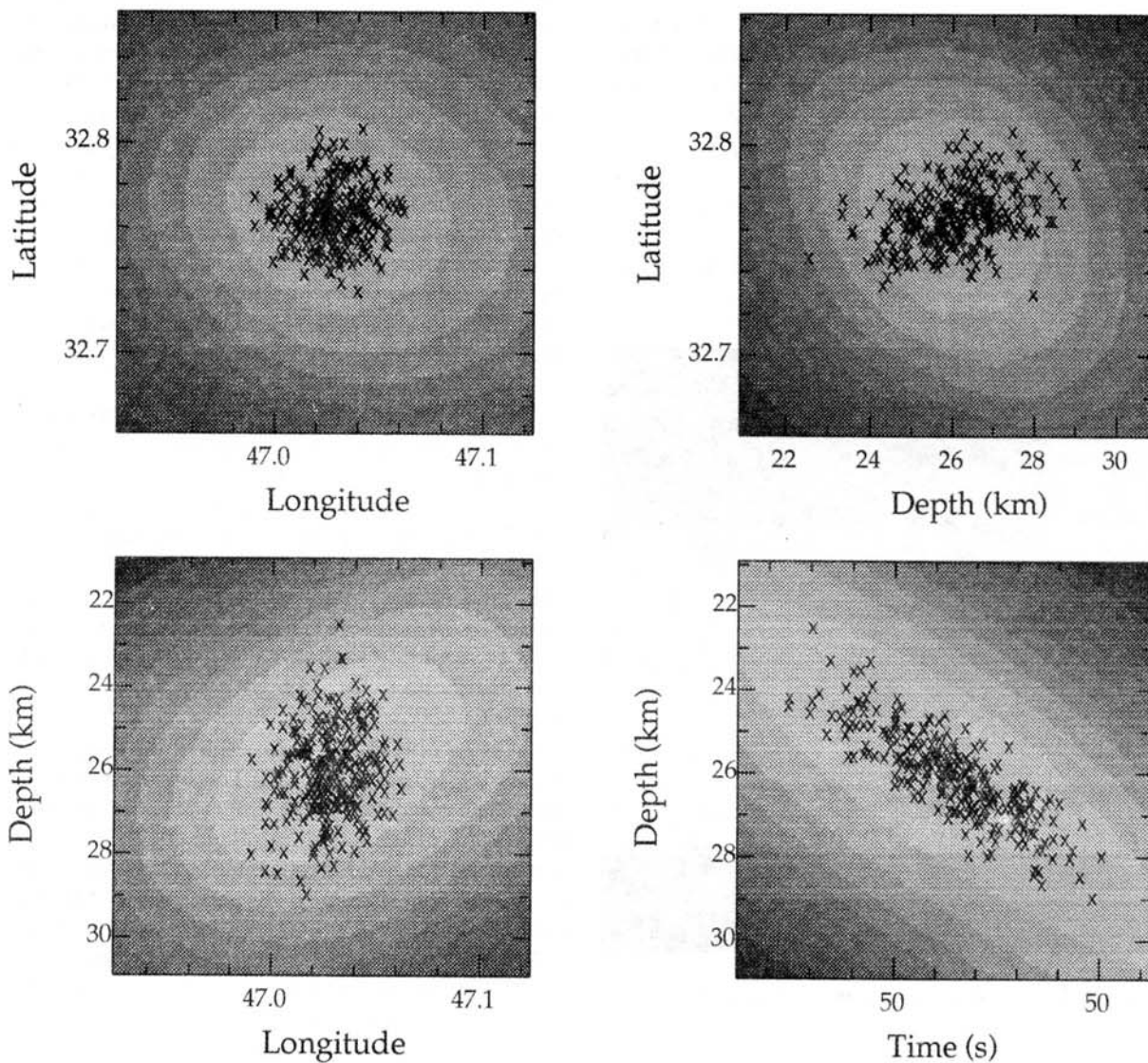Assuming that an earthquake occurred at $\mathbf{h} = (x, y,$



Figure 3. Misfit contours and distribution of perturbed locations for the Iran/Iraq earthquake using *P* and *pP* arrivals. The unperturbed location defines the center of each section. Lighter shading indicates lower misfit and hence *better* locations.

$z$, $t$) and ignoring picking errors, the observed arrival time at station $i$ will be

$$t_i^{arr} = t + t_i^{real}(x, y, z), \qquad (11)$$

where $t_i^{real}(x, y, z)$ is the travel time of the ray in the real Earth. Denoting the travel time through the *iasp*91 velocity model by $t_i^{syn}(x, y, z)$, the calculated arrival time at station $i$ will be given by

$$t_i^{calc} = t + t_i^{syn}(x, y, z). \qquad (12)$$

The residual at station $i$ is given by $res_i = t_i^{arr} - t_i^{calc}$. If $res_i > 0$, then $t_i^{real} > t_i^{syn}$, which means that the real travel time is greater than the calculated travel time, implying that waves in the real earth from $\mathbf{h}$ to station $i$ are slow relative to *iasp*91. Alternatively, if $res_i < 0$, the real travel time is fast relative to *iasp*91. If the proposed hypocenter $\mathbf{h}^{calc} = (x^c, y^c, z^c, t^c)$ differs from the real hypocentre $\mathbf{h}^{real}$, then other factors can cause the calculated and observed arrival times to differ. To force $res_i > 0$, i.e.

$$(t - t^c) + (t_i^{real}(x, y, z) - t_i^{calc}(x^c, y^c, z^c)) > 0, \qquad (13)$$

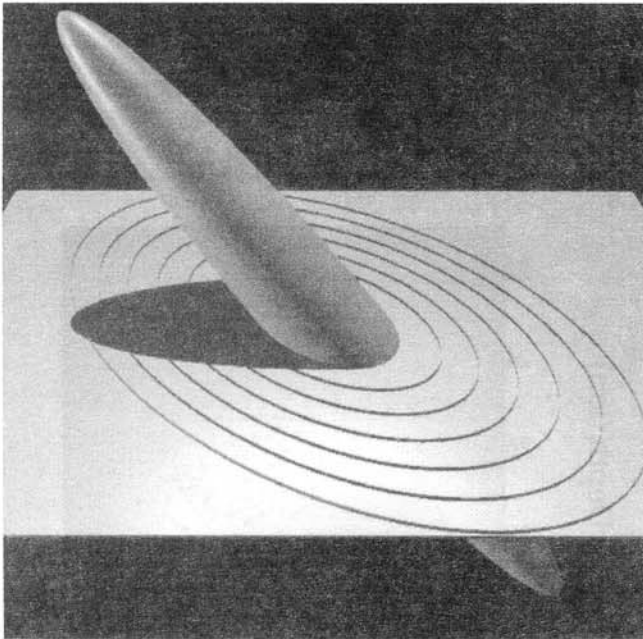the hypocenter must be moved so that the left-hand side



Figure 4.  Illustration of the projection effect in three dimensions. The ellipse represents a surface of constant functional value, $f^c$. On the reference plane are contours of this function. The shaded area represents the projection of all regions with functional value less than $f^c$. The projection of the ellipsoid and the function contours are oriented in completely different directions.

of equation (13) increases. This occurs if the calculated origin time, $t^c$ is decreased, or if $t_i^{calc}$ is decreased by moving the calculated epicenter toward the recording station, or by increasing the calculated depth of focus (for teleseismic events). In short, if $res_i > 0$, any of the following may apply: real rays are slow relative to *iasp*91, the epicenter is mislocated toward the station, the depth of focus is increased (for teleseismic events), and/or the origin time is decreased. For $res_i < 0$, the opposite is true. That is, the real rays are fast relative to *iasp*91, and/or the calculated epicenter is mislocated away from the station, and/or the depth is decreased (for teleseismic events), and/or the origin time is increased.

To illustrate the effect of magnitude dependence of location, events in the Flores Sea are considered. It is well known that paths to Australia from this region are fast relative to *iasp*91 (Bowman and Kennett, 1990, 1993). This means that rays traveling toward stations in Australia will travel faster than waves traveling toward stations in Europe and Asia. At low magnitudes, arrivals are mostly available from Australian stations, and because of the fast paths, the event will be dragged toward Australia. Higher-magnitude events will be recorded by larger numbers of Asian and other stations. In an inversion, the residuals at Australian stations are likely to be large, and will consequently have little effect on the solution as they are down weighted by the robust statistical norm. The location will then be dragged toward Asia and the calculated solution will depend on the magnitude of the earthquake.

Three station networks are used in the relocation. Each is based on the typical recordings of real events reported to the ISC (see Table 1). The first is a large magnitude 5.5 event that occurred on 21 March 1986. For this event, the ISC reported 201 observations, of which 190 are used here (130 stations). The second is a medium magnitude 4.9 event with 118 observations recorded by 74 stations. The third is a magnitude 4.4 event with 14 recording stations and 21 observations. The station distributions for each of the events are shown in Figure 6.

The relative locations for each of the three simulated events are listed in Table 2. The hypocenter of the intermediate-magnitude event differs only slightly from the hypocenter of the large-magnitude event. However, the low-magnitude event hypocenter has been pulled toward the Australian stations a distance of 8.5 km, has increased depth by 12.5 km, and decreased origin time by 0.7 sec. The fast paths to Australia are being compensated by moving the event toward the Australian stations and increasing the depth of focus. These both have the effect of decreasing the calculated travel time. In addition, the decrease in origin time reduces the discrepancy between calculated and observed arrival times. These effects combined to increase the LHS of equation (13) for Australian stations.

At low magnitudes, the earthquake is pulled toward Australia, because relative to *iasp*91 the Australian paths are fast, and there are not enough stations at other azimuths to counteract this effect. However, when additional stations are included, the residuals at Australian stations are large and down weighted by the robust statistical norm. This can be seen in Figure 7, which plots the residuals at each of the Australian stations used for all three locations. For the low-magnitude event, the residuals are either positive, or very small and negative. This is consistent with the event being pulled toward these stations. The two stations with negative residuals are to the southeast of the earthquake, partly away from the

southwesterly mislocation of the epicenter. For the intermediate- and large-magnitude locations, the residuals all become more negative, indicating that the influence of the Australian stations is being down weighted. When the same procedure is applied assuming the residuals follow a normal distribution, the locations are also found to be magnitude dependent. However, the mislocations are not systematic and are dominated by large residuals at a few stations. In conclusion, the use of a 1D velocity model and a robust statistical norm can lead to a systematic magnitude dependence of locations because of the variation in real velocity with azimuth about the earthquake.
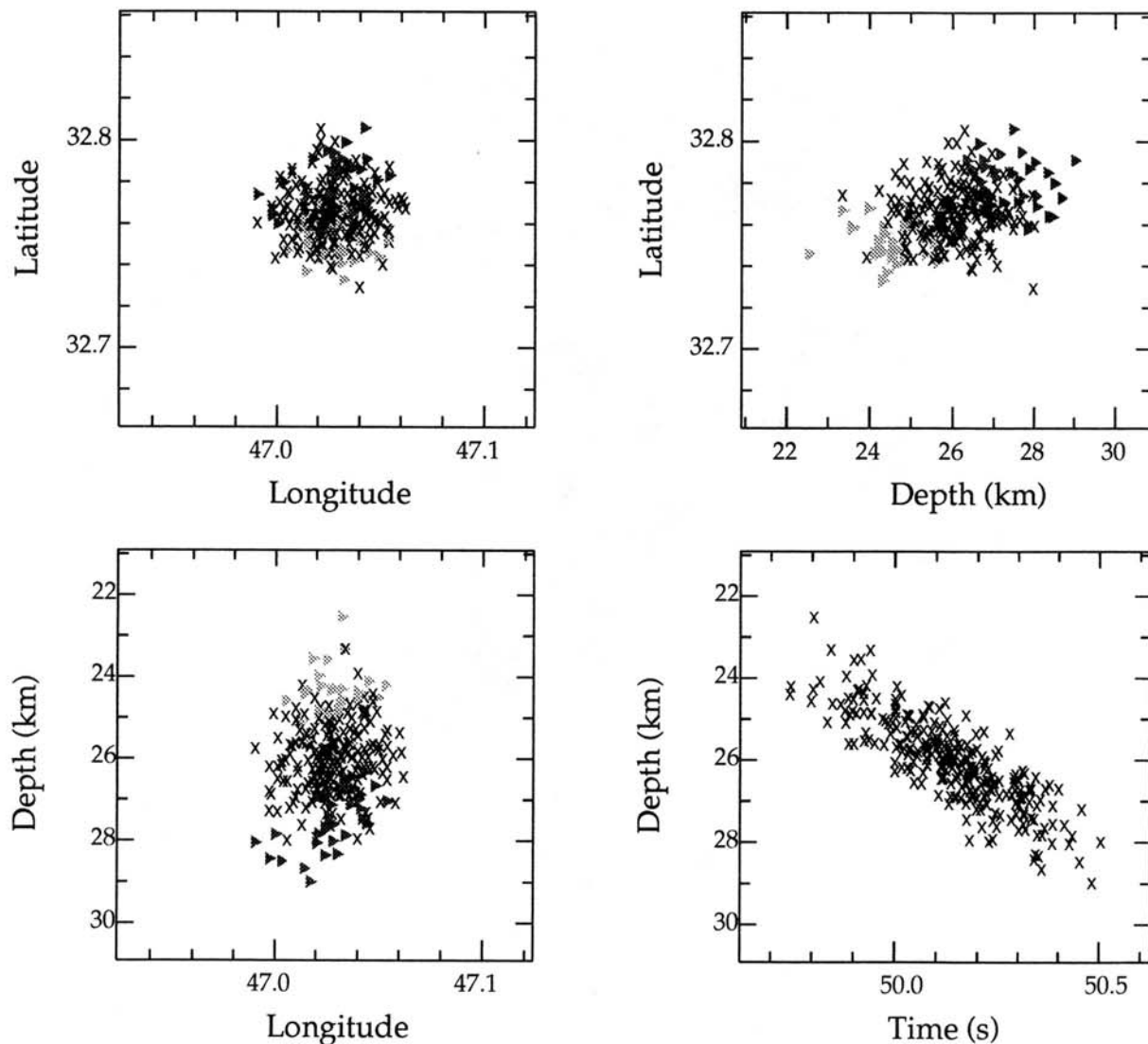


Figure 5.    The projection effect for the Iran/Iraq earthquake using *P* and *pP* arrivals. The misalignment of perturbed locations and misfit contours can be explained by a projection effect involving origin time. Dark triangles: locations with origin times 0.3 sec or more larger than the unperturbed origin time. Light triangles: 0.3 sec or more less. Crosses: All other locations.

## Discussion and Conclusions

Monte Carlo analysis has indicated that for the Iran/Iraq event, picking errors do not move the calculated hypocenter by more than 4.5 km in epicenter and 6 km in depth. These errors are significantly smaller than the difference between the location found using only $P$ arrival time data and the one that uses both $P$ and $pP$ data (i.e., 12.5 km in epicenter and 35 km in depth). On a large subset of events, the effect on the hypocenter from velocity-model errors was generally found to be significantly larger than the effect of picking errors. However, when multiple local and regional arrivals of $P$ were available, the depth could be resolved accurately using $P$ arrivals only. In addition, for events with stations all to one side of the epicenter, the location was extremely unstable to changes in the arrival times. In that case, the picking errors alone can move the epicenter by more than 100 km and the depth by more than 50 km. We agree with previous authors (e.g., Van der Hilst and Engdahl, 1993) for the need to use multiple arrivals, especially depth-sensitive phases such as $pP$, to accurately constrain the focal depths of teleseismic events (see also Van der Hilst and Engdahl, 1992), and also find that, in general, the most important component of error seems to be due to the velocity model.

In our example, the Monte Carlo treatment of picking errors alone is insufficient to highlight the true mislocation of the event when it is based only on $P$ arrival times. We believe that changing the nature of the constraint on the data; i.e., by including independent data of a different type, is a much more powerful way of



Figure 6. Station distribution for the three Flores events. Stations marked by an open diamond recorded arrivals during the low-magnitude event. Additional stations that recorded arrivals for the medium (filled triangles) and large (filled hexagons) events are also shown.
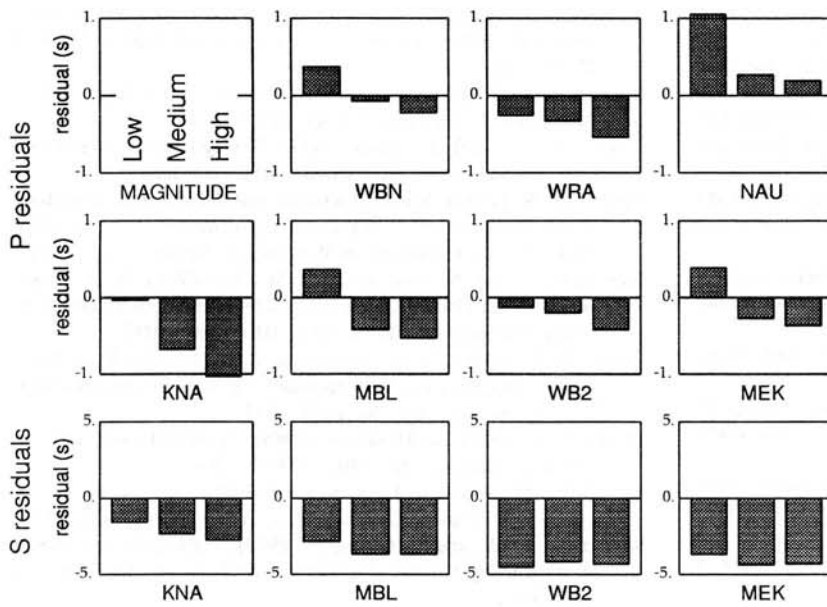
Figure 7. Residuals at Australian stations that recorded all three events. For the low-magnitude event, the residuals are either positive, or very small and negative. For the intermediate- and large-magnitude locations, the residuals all become more negative, indicative of the fact that the event is dragged away from Australia.

Table 2
The Relative Locations for the Large-, Intermediate-, and Low-Magnitude Flores Events (The additional Row after the Intermediate- and Low-Magnitude Events Represents the Movement of These Hypocenters Relative to the Large-Magnitude Event)

| Event | Latitude | Longitude | Depth | Origin Time |
|---|---|---|---|---|
| Flores (large) | 7.495° S | 120.635° E | 622.4 km | 37.9 |
| Flores (medium) | 7.491° S | 120.648° E | 619.9 km | 37.6 |
| | 0.4 km N | 1.4 km E | −2.5 km | +0.25 sec |
| Flores (small) | 7.559° S | 120.592° E | 609.7 km | 37.2 |
| | 7.1 km S | 4.8 km W | +12.7 km | −0.7 sec |

assessing the true mislocation of the event. Indeed, it seems likely that an attempt to take account of velocity-model errors by incorporating them into the Monte Carlo analysis would be futile, because the true nature of velocity-model errors cannot adequately be described by some simplistic statistical distribution. In our examples, and we believe in more general cases as well, it will always be better to try and alter the information content of the data, perhaps by including phases such as $pP$, than to rely on a large number of $P$ arrivals and the most sophisticated error analysis available.

The use of a 1D velocity model to calculate travel times can lead to the location of an event becoming magnitude dependent. At different magnitudes, the arrival types and recording stations differ. The errors introduced by the velocity model vary with the different station geometries and phase combinations. Consequently, in regions with large lateral variations of seismic velocities, hypocenters calculated using these distinct station geometries and phase assemblies can vary significantly. In particular, it was found that for events in the Flores Sea, the fast paths to Australia have the effect of dragging low-magnitude events toward the Australian stations, because few stations at other azimuths record arrivals. For larger magnitudes, however, many Asian and European stations record arrivals and so the residuals at Australian stations become large and are down weighted, and the event is then dragged back toward Asia. This leads to a significant magnitude-dependent mislocation of the earthquake, which may well be a common effect in other teleseismic earthquake locations.

## Acknowledgments

## References

Adams, R. D., A. A. Hughes, and D. M. McGregor (1982). Analysis procedures at the International Seismological Centre, *Phys. Earth Planet. Interiors* **30**, 85–93.

Anderson, K. R. (1982). Robust earthquake location using M estimates, *Phys. Earth. Planet. Interiors* **30**, 119–130.

Billings, S. D. (1994). Simulated annealing for earthquake location, *Geophys. J. Int.* **118**, 693–706.

Billings, S. D., B. L. N. Kennett, and M. S. Sambridge (1994). Hypocentre location: genetic algorithms incorporating problem specific information, *Geophys. J. Int.* **118**, 680–692.

Bowman, J. R. and B. L. N. Kennett (1990). An investigation of the upper mantle beneath NW Australia using a hybrid seismograph array, *Geophys. J. Int.* **101**, 411–424.

Bowman, J. R. and B. L. N. Kennett (1993). The velocity structure of the Australian shield from seismic travel times, *Bull. Seism. Soc. Am.* **83**, 25–38.

Buland, R. (1976). The mechanics of locating earthquakes, *Bull. Seism. Soc. Am.* **66**, 173–187.

Davies, J. H. (1992). Lower bound estimate of average earthquake mislocation from variance of travel time residuals, *Phys. Earth Planet. Interiors* **75**, 89–101.

Evernden, J. F. (1969). Precision of epicentres obtained by small numbers of world-wide stations, *Bull. Seism. Soc. Am.* **59**, 1365–1398.

Feldman, D. and M. Fox (1991). *Probability: The Mathematics of Uncertainty*, Marcel Dekker, New York.

Flinn, E. A. (1965). Confidence regions and error determinations for seismic event location, *Rev. Geophys.* **3**, 157–185.

Hoel, P. G. (1971). *Introduction to Mathematical Statistics*, Wiley, New York.

Jeffreys, H. (1932). An alternative to the rejection of observations, *Proc. R. Soc. London A* **137**, 78–87.

Jordan, T. H. and K. A. Sverdrup (1981). Teleseismic location techniques and their applications to earthquake clusters in the south-central Pacific, *Bull. Seism. Soc. Am.* **71**, 1105–1130.

Kennett, B. L. N. (1992). Locating oceanic earthquakes—the influence of regional models and location criteria, *Geophys. J. Int.* **108**, 848–854.

Kennett, B. L. N. and E. R. Engdahl (1991). Traveltimes for global earthquake location and phase identification, *Geophys. J. Int.* **105**, 429–465.

Kennett, B. L. N. and M. S. Sambridge (1992). Earthquake location: genetic algorithms for teleseisms, *Phys. Earth Planet. Interiors* **75**, 103–110.

Kirkpatrick, S. C., D. Gelatt, and M. P. Vecchi (1983). Optimization by simulated annealing, *Science* **220**, 671–680.

Lawson, C. H. and R. J. Hanson (1974). *Solving Least Squares Problems*, Prentice-Hall, Englewood Cliffs, New Jersey.

Leaver, D. S. (1984). Mixed stochastic and deterministic modelling of the crustal structure in the vicinity of Mount Hood, Oregon, *Ph.D. Thesis*, University of Washington, Seattle, Washington.

Metropolis, N., M. N. Rosenbluth, A. W. Rosenbluth, A. H. Teller, and E. Teller (1953). Equation of state calculations by fast computing machines, *J. Chem. Phys.* **1(b)**, 1087–1092.

Pavlis, G. L. (1986). Appraising earthquake hypocenter location errors: a complete, practical approach for single event locations, *Bull. Seism. Soc. Am.* **76**, 1699–1717.

Pavlis, G. L. and N. B. Hokanson (1985). Separated earthquake location, *J. Geophys. Res.* **90**, 12777–12789.

Sambridge, M. S. and B. L. N. Kennett (1986). A novel method of hypocentre location, *Geophys. J. R. Astr. Soc.* **87**, 679–697.

Sambridge, M. S. and K. Gallagher (1993). Earthquake hypocenter location using Genetic Algorithms, *Bull. Seism. Soc. Am.* **83**, 1467–1491.

Tarantola, A. and B. Valette (1982). Inverse problems—quest for information, *J. Geophys.* **50**, 159–170.

Van der Hilst, R. D. and E. R. Engdahl (1993). Step wise relocation of ISC earthquake hypocentres for linearised tomographic imaging of slab structure, *Phys. Earth Planet. Interiors* **75**, 39–54.

Research School of Earth Sciences
Institute of Advanced Studies
Australian National University
Canberra, Australia